

Nested sequences of period-adding stability phases in a CO₂ laser map proxy

José R.B.M. Araújo^{a,b}, Jason A.C. Gallas^{a,b,c,*}

^a Departamento de Física, Universidade Federal da Paraíba, João Pessoa 58051-970, Brazil

^b Instituto de Altos Estudos da Paraíba, Rua Silvino Lopes 419-2502, João Pessoa 58039-190, Brazil

^c Complexity Sciences Center, 9225 Collins Avenue Suite 1208, Surfside FL 33154, USA

ARTICLE INFO

Article history:

Received 10 May 2021

Accepted 10 June 2021

Keywords:

Period-adding

CO₂ laser

Hénon map

Nested periodicity

Phase diagrams

Parameter space

ABSTRACT

We report the discovery of wide nested sequences of period-adding complexification routes spanning the whole control parameter space of the Hénon map, a *discrete-time* proxy of single-mode loss-modulated CO₂ lasers. For a realistic map, the new adding routes found reproduce analogous phenomena previously observed in *continuous-time* differential equations describing, for instance, oscillatory phases in an enzyme reaction model. In contrast to differential equations, the map is analytically tractable to a large extent, and provides a prototypic framework to investigate intricate features of generic dissipative flows.

© 2021 Elsevier Ltd. All rights reserved.

1. Introduction

Period doubling and period adding are two familiar routes to complex dynamical behaviors in dissipative physical systems, the latter more elusive than the former [1–4]. Adding phenomena were observed experimentally as far back as 1927 by van der Pol and van der Mark [5,6]. In 1990, Levi [7] studied period adding generated by a circle map and outlined how the phenomenon arises for a whole class of van der Pol-type systems under periodic forcing. He also argued that the noise observed in the van der Pol system can be explained by the appearance of Hénon-like attractors. The dynamics of these electronic circuits is governed by differential equations, i.e. by continuous-time models [1–4].

More recently, series of unexpected nested spike-adding cascades were found in the stability phases of Olsen's enzyme reaction model, which describes the concentration of chemicals responsible for the enzyme reaction [8]. Remarkably, Olsen's model involving just four coupled differential equations and nine control parameters was found to reproduce well features known to be characteristics of a sophisticated state-of-the-art model of the reaction [9,10], involving ten coupled equations and fourteen rate constants. Periodicity in Olsen's flow was found to be prevalent over chaos. A number of regularities were reported, in particular unexpected nested sequences of period-adding stability phases.

Fig. 1 shows a representative example of a parameter window containing nested spike-adding colorful sequences of stability phases computed for Olsen's flow. From this figure one recognizes that stability phases accumulate in several different ways, extending as far as the eye can discern. The characteristic signature underlying Fig. 1 is that the stability phase with largest volume between the phases with 4 and 5 spikes is a 9-spikes phase, the largest phase between 9 and 4 spikes contains 13 spikes, etc.

The purpose of this paper is to report the observation of a nested *period-adding* phenomenon in a mapping, a discrete-time analog of the nested *spike-adding* scenario observed in Olsen's flow. Note that discrete-time dynamical systems do not display spikes and this is the reason for the distinct name. We found period-adding in a familiar and well-studied discrete-time dynamical system, namely the two-dimensional *smooth* dissipative Hénon map which, among other things, is a discrete-time proxy of single-mode loss-modulated CO₂ lasers [13–16]. More specifically, we report detailed stability charts for the weak dissipative $|b| \rightarrow 1$ Hamiltonian limits of the Hénon map

$$x_{t+1} = a - x_t^2 + by_t, \quad y_{t+1} = x_t. \quad (1)$$

Interesting results regarding period-adding in piecewise *non-smooth* maps having two discontinuities have been reported by Tramontana et al. [17], and in the references therein. In sharp contrast, the Hénon map studied here is smooth and has no critical points [18].

The Hénon map ranks among the most widely studied systems which exhibit strange attractors and chaotic behaviors. It was orig-

* Corresponding author.

E-mail address: jason.gallas@gmail.com (J.A.C. Gallas).

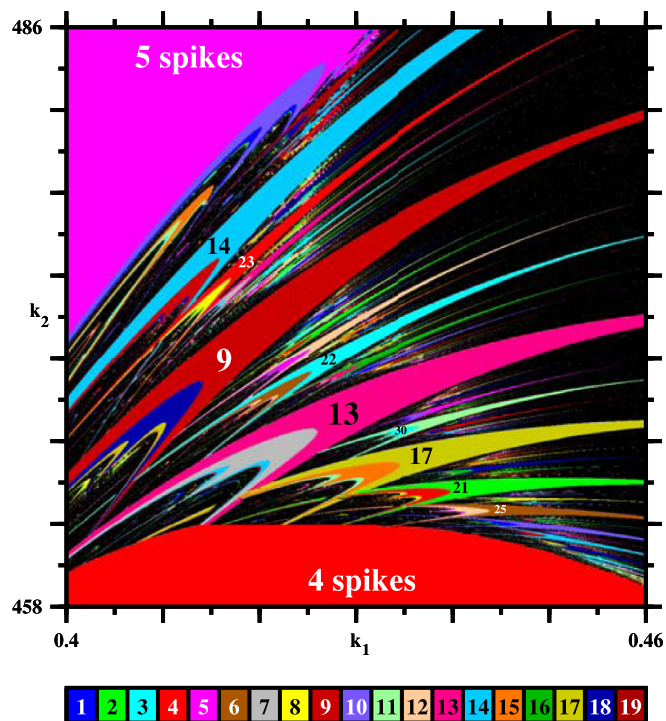


Fig. 1. Spike-adding sequences of stability phases observed in a the k_1 and k_2 control plane of a flow system, namely in the differential equations of Olsen's enzyme reaction [8]. Black denotes chaos, colors indicate periodic oscillations. The phase with largest volume between the phases with 9 and 4 spikes contains $9 + 4 = 13$ spikes, then $13 + 4 = 17$, $17 + 4 = 21$ spikes, etc extending as far as the eye can discern. For selected phases, numbers indicate the number of spikes (local maxima) per period of the oscillations, plotted recycling colors modulo 19. This figure displays 1200×1200 parameter points.

inally introduced as a simplified version of the celebrated Lorenz 1963 model of atmospheric convection [1–4]. The map was found to reproduce strikingly well stability diagrams obtained from differential equations representing the standard four-level model of a CO₂ laser with modulated losses [13–16]. For a recent survey see, e.g. Ref. [19]. Appealing physical interpretations of Hénon's map were given by Heagy [20]. The control parameter space of the map is known to display several regularities [11]. Additional properties of the Hénon map were also extensively discussed in the last publication of Lorenz [21], considered one of the *founding fathers* of chaos theory [22]. Before starting, we mention that the Hamiltonian limit was already explored for another familiar map, namely for a kicked rotor [23].

Theoretically, a startling novelty is to observe the ubiquitous presence of adding-cascades in a system with no critical points [18], which are normally used to classify stability properties of dynamical systems [1–4]. The dissipation strength in Eq. (1) is controlled by the Jacobian $-b$, which varies in the interval $-1 \leq b \leq 1$. Stability charts are already available [11] for the region of strongest dissipation, roughly long the stripe $-0.6 \leq b \leq 0.8$. In this region one finds a wide chaotic phase containing many regularities embedded in it like, e.g. *shrimp cascades* [11,21]. As it may be seen from Figs. 1–3 in Ref. [11], the wide phase of chaos, the white region seen here at the center of Fig. 2, is crisscrossed by numerous long and narrow stripes of stable periodic oscillations whose origin and organization does not seem to have been ascertained yet. As shown below, we find such narrow stripes to originate from the Hamiltonian limits of the map, namely from the limits $b \rightarrow \pm 1$. Therein lies the rub: These limits are notoriously difficult to handle because the vanishing dissipation implies an ever growing multistability and a large increase of the transient times needed to reach

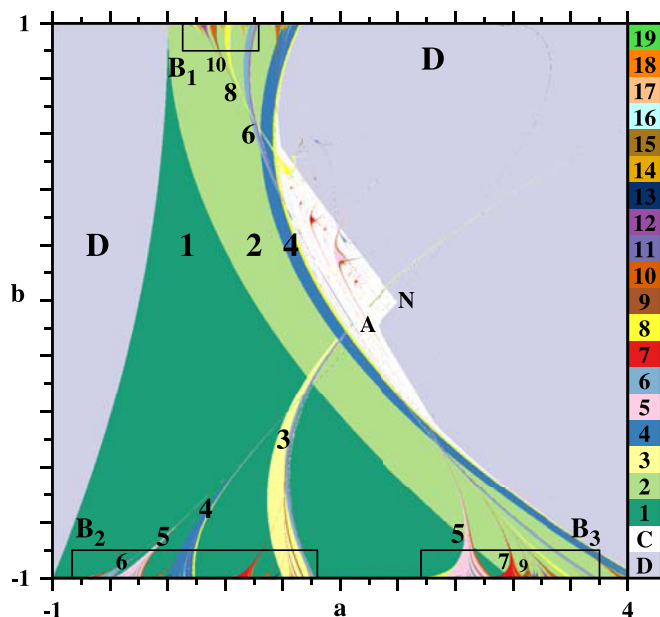


Fig. 2. Period-adding cascades of the Hénon map, issuing from the three boxes B_1, B_2, B_3 , shown magnified below in Figs. 3 and 4. Colors represent stability phases with numbers indicating the periodicity of some of the larger individual phases. White indicates chaos while D marks parameters leading to divergence. N and A refer to the *nose* and *antinose* [11,12], the two apparently sharp vertices on the outer boundary of the phase of chaos. Periods are plotted recycling colors modulo 19 (see text). Each panel displays the analysis of 1200×1200 parameter points.

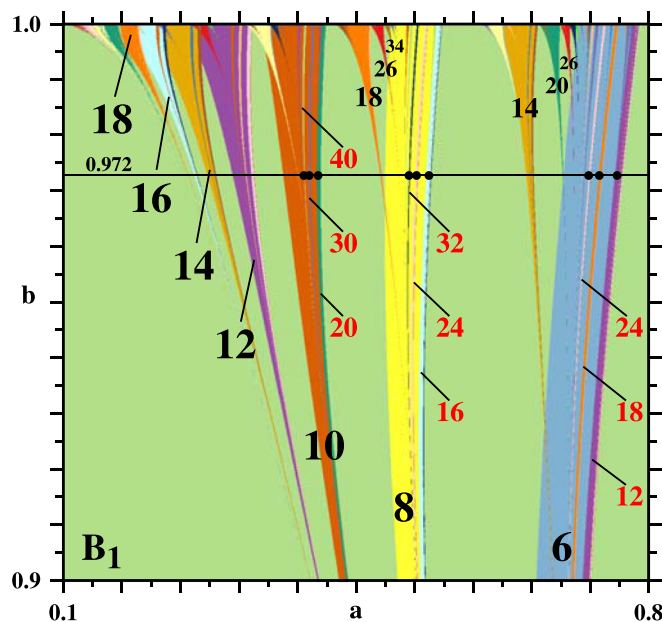


Fig. 3. Magnification of the box B_1 seen in Fig. 2, illustrating nested period-adding sequences near $b = 1$. Red numbers refer to substripes embedded in larger stripes. Apparently, this box contains only even periods. This figure displays the analysis of 1200×1200 parameter points. Basins of attraction for the three sets of three points along the line $b = 0.972$ are shown below in Fig. 5. The color coding is the same as in Fig. 2. (For interpretation of the references to color in this figure legend, the reader is referred to the web version of this article.)

and distinguish asymptotic attractors unambiguously. The Hamiltonian limit is where every initial condition turns into an individual attractor and, therefore, where the number of attractors grows without bound [23–25].

Before proceeding, we mention that parameter charts with various degrees of accuracy and covering the full range $-1 \leq b \leq 1$ are

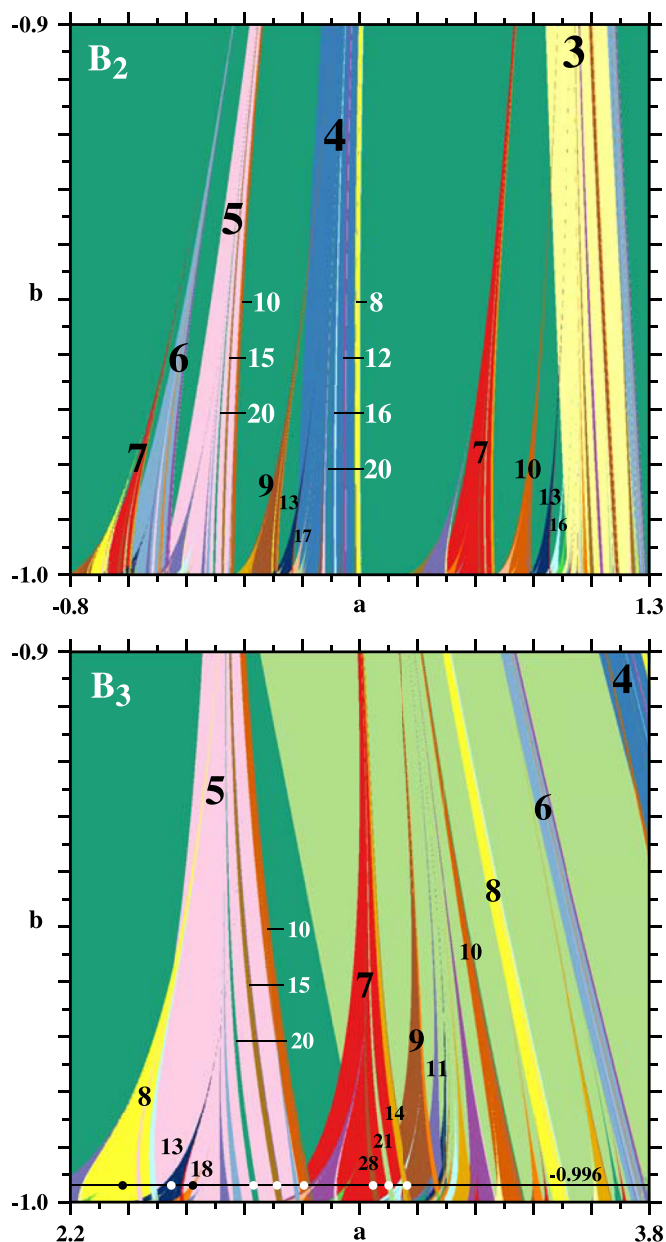


Fig. 4. Magnification of boxes B_2 and B_3 in Fig. 2, illustrating nested sequences of period-adding cascades near $b = -1$. White numbers refer to substripes (see Section 2). Each panel displays the analysis of 1200×1200 parameter points. Basins of attraction for the three sets of three points along the line $b = -0.996$ are shown below in Fig. 6. The color coding is the same as in Fig. 2.

available in the literature, for instance in Refs. [26–28]. However, they consider at most periods $k = 7$. Below we report systematic results for substantially larger periods.

2. Period-adding in the Hénon map

Fig. 2 shows a global view of the control parameter space of the Hénon map, indicating with colors the main features present in this phase diagram. The regions of premier interest to us are basically those contained in the three boxes B_1 – B_3 shown magnified below in Figs. 3 and 4. As in Ref. [11], colors in these figures refer to the asymptotic periodicity of the oscillations recorded for each point (a, b) . In Figs. 2–4, the $a \times b$ control plane is seen to be riddled with multistability, namely with stripes or, equivalently, with phases displaying the overlap of two or more colors, a clear

indication of the existence of more than one stable asymptotic oscillation for a given parameter point (a, b) . To increase the information content of the phase diagram, in presence of multistability, the solution plotted in Fig. 2 (and all other ones below) is the one having the smallest basin of attraction in the parameter window considered. The smallest the basin, the higher the period.

The orbital periodicity is plotted on a discrete grid containing 1200×1200 equally spaced points (a, b) . For each point (a, b) , up to $150 \times 150 = 22,500$ initial conditions (x_0, y_0) covering suitable regions in phase-space were iterated for Eq. (1). In this way, basins of attraction and histograms classifying all coexisting orbits are produced. The largest period k found was then used to color the point (a, b) in Fig. 2, according to the color table shown in the figure. Orbits having periods $k > 19$ are represented modulo 19, namely by periodically recycling the 19 colors shown in the color table in the figure. Since the relative size of basins of attraction varies when parameters are changed, it was sometimes necessary to use finer initial conditions grids. For instance, near the non-dissipative limits $|b| = 1$, grids containing up to $400 \times 400 = 1.6 \times 10^5$ initial conditions were considered. The investigation of the Hamiltonian limit is a computer intensive task, due to the significant increase of transients and multistability as $|b| \rightarrow 1$.

As may be seen from Fig. 2, period-doubling cascades emerge to the right of the large period-one stability phase, in the direction of increasing a . In addition to such phases characterized by period doubling, it is also possible to see many additional phases with the form of triangular stripes, originating from both limits $b = 1$ and $b = -1$. Each such phase has an individual period-doubling cascade which, however, becomes thinner and thinner very fast when a increases. A clear regular pattern in the organization of these triangular phases emerges when one considers as a reference point their leftmost points (the smaller a) along the $|b| = 1$ lines. For example, looking at the bottom of Fig. 2, one sees that: i) The largest stability phase between the period-one and -two is a phase with period $k = 1 + 2 = 3$. ii) The largest stability phase between the period-one and -three is a phase with period $k = 3 + 1 = 4$. iii) The largest stability phase between of period-one and -four is a phase with period $k = 4 + 1 = 5$, and so on. Although in these examples one of the reference phases was always the period-one phase, the same rule remains valid for any arbitrary pairs of phases. For instance, on the top of Fig. 2 the largest phase between periods four and two has period $k = 4 + 2 = 6$. The period-ten phase is the largest one between period-eight and period-two phases, and so forth.

Figs. 3 and 4 show magnifications of the boxes B_1 – B_3 in Fig. 2. From Figs. 3 and 4 one recognizes that the period-adding rule applies in general, namely that the largest stability phase between phases with periods k_1 and k_2 is a phase with period $k = k_1 + k_2$. This is the main message of this paper: period-adding cascades exist in profusion in the Hénon map.

As the period increases, notice that the phases start to overlap significantly and to converge to some accumulation point on the lines $|b| = 1$. This makes visualization of the reference points of overlapping phases relatively difficult because, as explained above, the pictures are colored according to the orbit with largest periodicity. This overlapping between “main” phases is not to be confused with the overlapping of “subphases” and their corresponding main phases. We call subphases the structures that emerge between the reference point of a main phase and the reference point of the period-doubled phase that originates from it. Their periods are marked with red numbers in Fig. 3 and with white numbers in Fig. 4.

While two main phases may overlap only partially, a subphase is always contained entirely within its main phase. Although not visible in Fig. 2, subphases within a main phase may overlap each other as their period increases and they accumulate. Furthermore,

they also undergo a period-doubling cascade process, presenting “sub-subphases”. This organization scheme, as well as the period-adding rule, may be recognized at all “levels” in the control parameter space. An interesting open question is to determine whether or not the number of period-added phases is finite or not. To conclude this section, we mention that it is possible to define rotation numbers and to use them to establish a hierarchical structure among stability phases, similar to the hierarchy known for the Mandelbrot set. These results, however, are beyond the scope of the present work and will be reported elsewhere.

3. Basin of attraction in the Hamiltonian limits

Phase diagrams like the ones in Figs. 2–4 are usually computed by “following the attractor”, namely by starting numerical integrations from some selected parameters and using the numerical

values of the variables obtained at the end of an integration as the initial values to start new calculations after incrementing a parameter of interest. This procedure tends to select initial conditions from a fixed basin of attraction, normally the basin with largest volume in phase space. However, this procedure does not work if one wishes to compute phase diagrams close to the Hamiltonian limit. That this is so may be appreciated from Figs. 5–7.

Fig. 5 presents a representative illustration of the changes undergone by the basins of attraction when a increases along a fixed (and arbitrary) value of b inside box B1, viz. $b = 0.972$. Basin colors were selected to maximize contrast in the figures and may differ from the colors used in Figs. 2–4. As seen from Fig. 2, along this line the period-adding cascades unfold against a background of period-two orbits. Therefore, to be able to display the period-adding cascades, we avoid plotting period-two orbits, and plot orbits with suitably higher periods. As one moves from $a = 0.401$

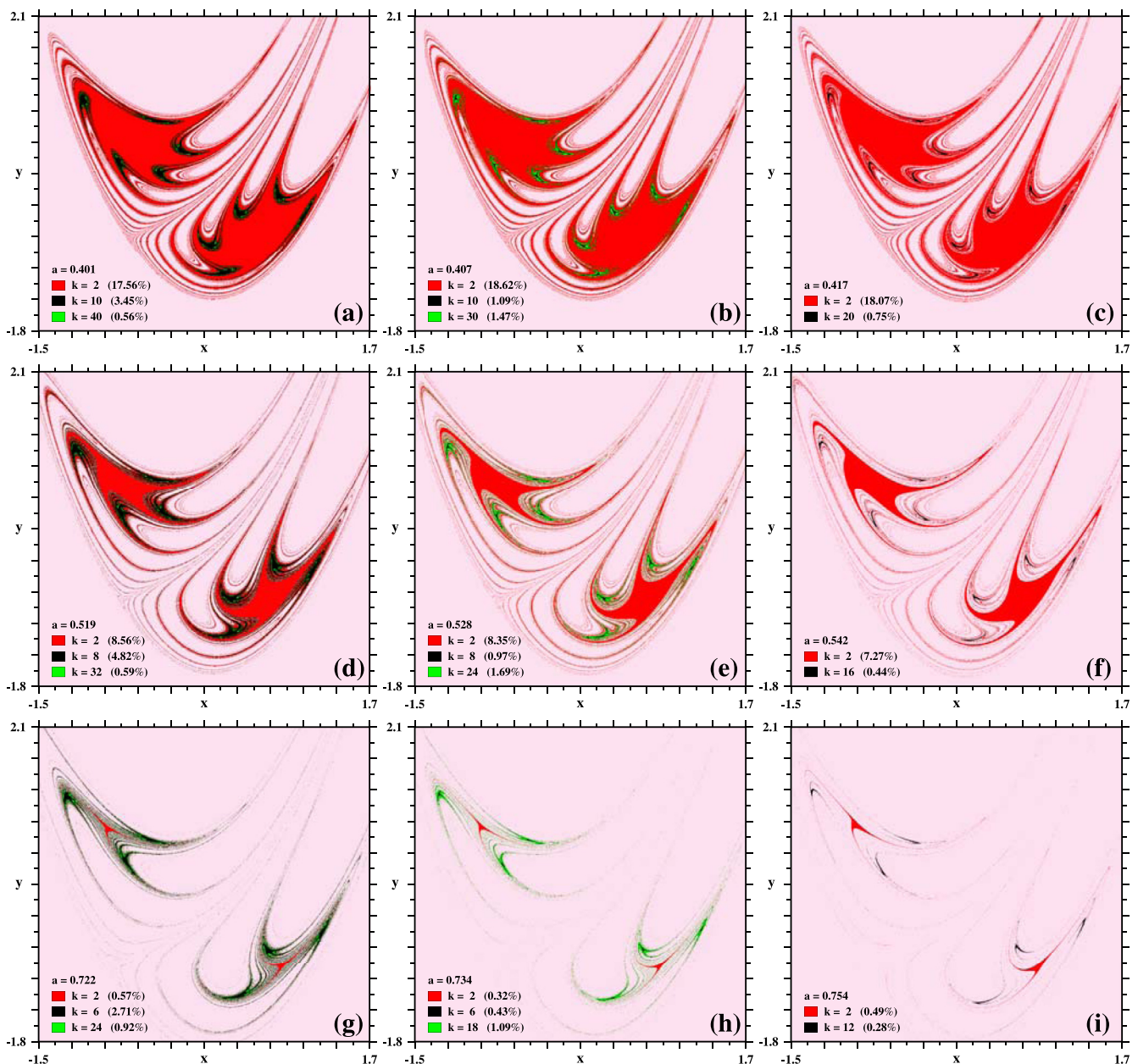


Fig. 5. Illustrative example of the steady decrease of basin volume when a increases along the line $b = 0.972$, shown in Fig. 3. The orbital periods and corresponding basin volumes are indicated inside the individual panels. The pink background denotes initial conditions leading to the attractor at infinity (divergence). (For interpretation of the references to color in this figure legend, the reader is referred to the web version of this article.)

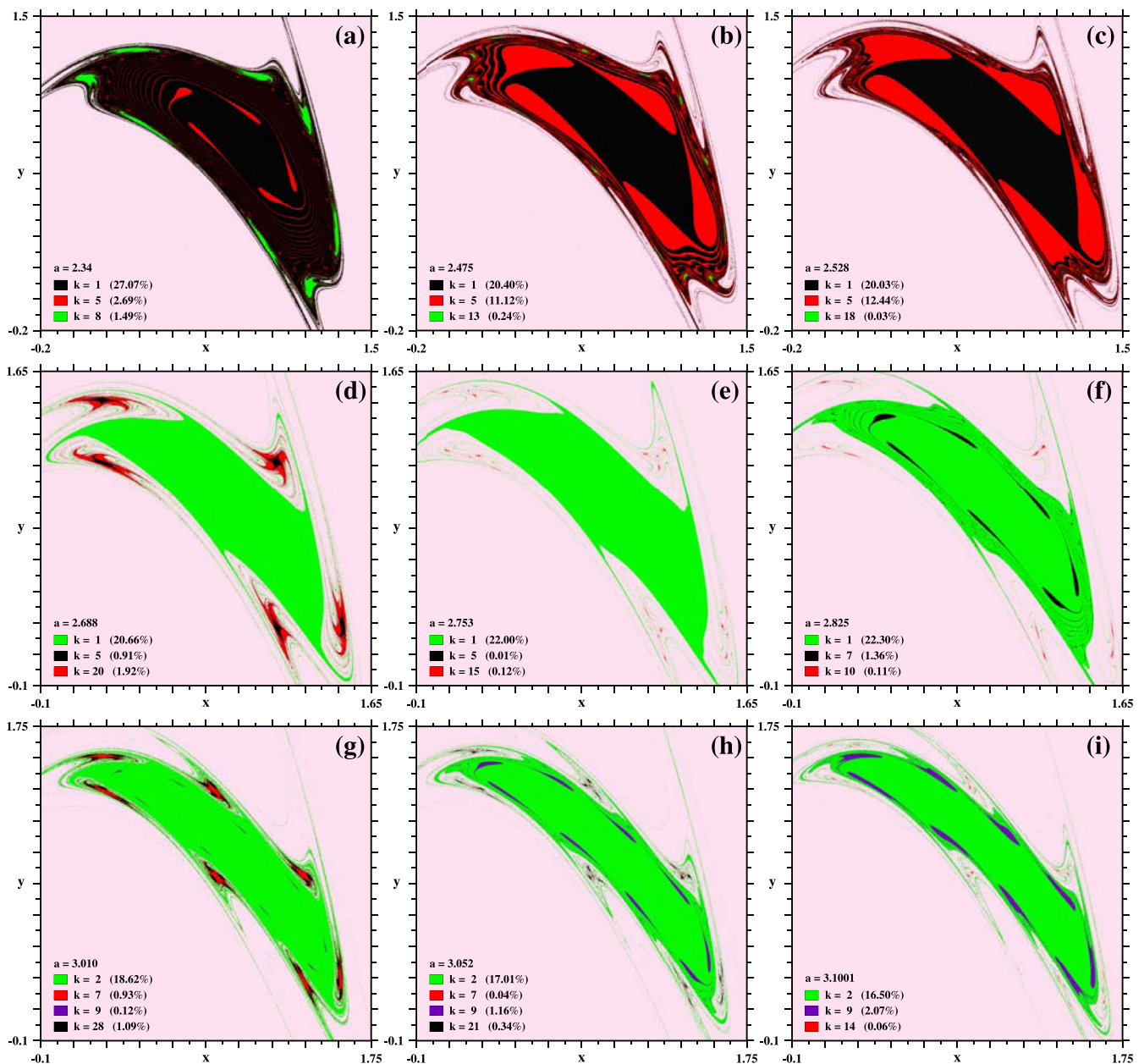


Fig. 6. Illustrative example of the attractor variation as a increases along the $b = -0.996$ line, indicated in box B3 in Fig. 4. The orbital periods and corresponding basin volumes are indicated inside the individual panels. The pink background denotes initial conditions leading to the attractor at infinity (divergence). (For interpretation of the references to color in this figure legend, the reader is referred to the web version of this article.)

(Fig. 2(a)) to the last panel for $a = 0.754$ (Fig. 2(i)), there is a strong reduction of the volume of all basins, e.g. the period-two basins decreases from 17.56% to 0.49%. The basin of the unbounded attractor at infinity (divergences) grows substantially, something that seems counterintuitive when contemplating the large and smooth extension of the period-one and period-two phases in Fig. 2. Thus, one sees that extra care is needed to make sure to select and plot the relevant basins in order to display the period-adding cascade.

Fig. 6 shows basins of attraction for nine values of a along the line $b = -0.996$, inside box B3 in Fig. 4. Despite the fact that the magnitude of b is now much closer to 1 than in Fig. 5, the basin volumes remain much more constant, in sharp contrast to what is seen in Fig. 5. When compared with Fig. 5, the main changes occur in the periods and shapes of the basins which coexist with periods one and two. While these two basin keep their volumes relatively constant, the volume of the basins embedded in them vary con-

siderably. Although all basins in Figs. 5 and 6 are clearly fractal, the period-two “core” of the basins in Fig. 6(d) and (e) are smooth, with fractality showing up only as outer filaments. In other words, their cores do not contain other basins embedded in them.

Finally, Fig. 7 shows successive magnifications of the basin obtained for $a = -0.44$ and $b = -0.99999$, a magnitude much closer to 1 as before. The individual panels were computed after discarding 2.7×10^6 initial iterates, regarded as transient needed to come close to the asymptotic attractors. An exception is Fig. 7(f) where transients of 4×10^6 initial iterates were discarded. As it is clear from this figure, the number of distinct attractors seems to be growing without bound as $b \rightarrow -1$. Indeed, in this limit the basins of attraction already show great similarity with the familiar phase-space diagrams of Hamiltonian systems. Again, this behavior seen in Fig. 7 emphasizes the need for special care when following the impact of parameter changes in this complex limit.

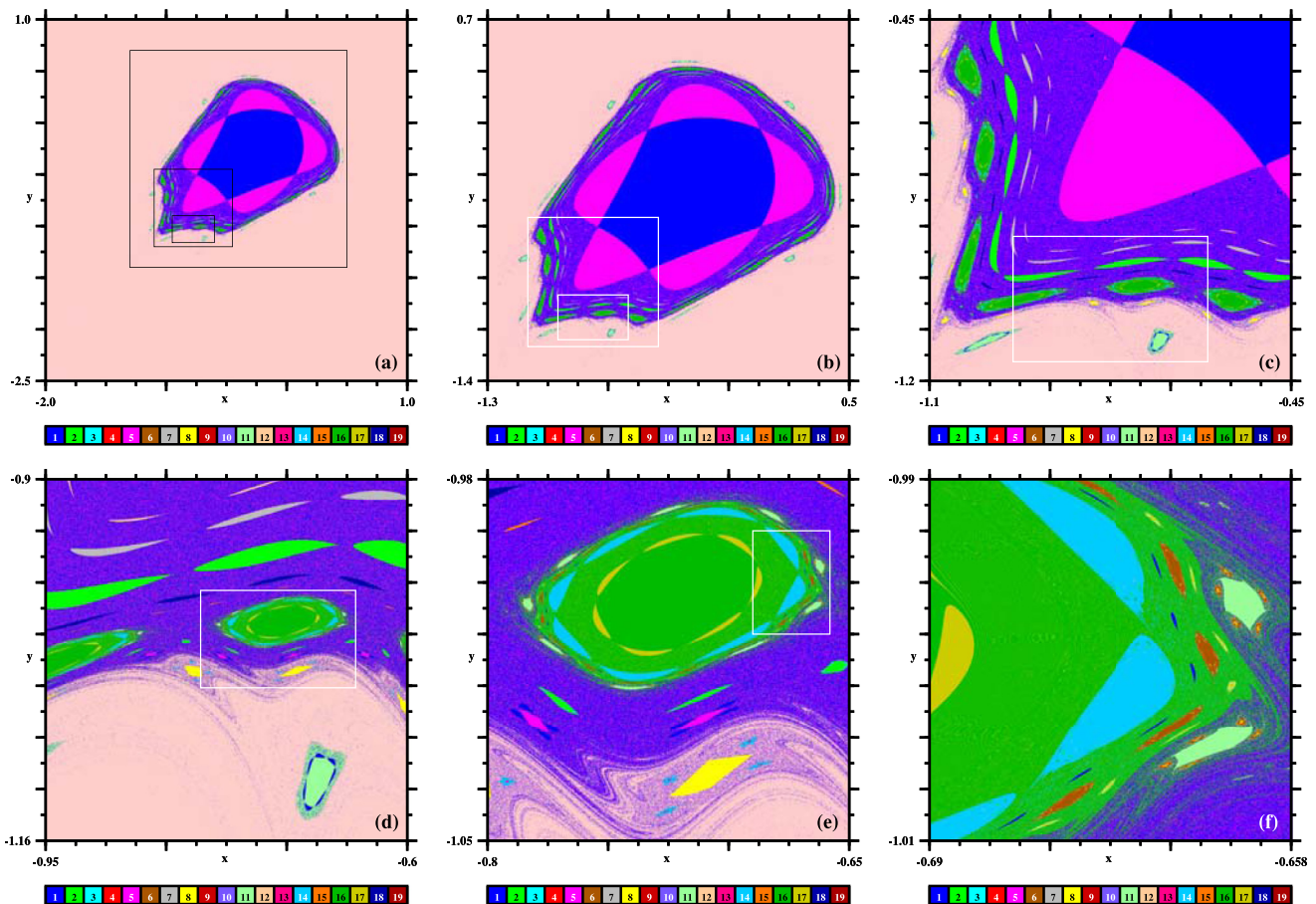


Fig. 7. Successive magnifications illustrating the unbounded growth of the number of distinct attractors when approaching the Hamiltonian limit, here for $a = -0.44$ and $b = -0.99999$. Each panel show results of the analysis of a grid containing $1200 \times 1200 = 1.44 \times 10^6$ initial conditions. The pink background denotes initial conditions leading to divergence. (For interpretation of the references to color in this figure legend, the reader is referred to the web version of this article.)

4. Conclusions and outlook

In summary, this work describes the discovery of wide nested sequences of period-adding complexification routes spanning the control parameter space of the Hénon map, a *discrete-time* proxy of single-mode loss-modulated CO₂ lasers. For a realistic and smooth map, the new adding routes being reported reproduce analogous phenomena observed previously in *continuous-time* differential equations which describe, for instance, the oscillatory phases of an enzyme reaction model. All structures described in this work are *stability* phases and, therefore, are directly accessible to experimental observation. While period-doubling has been extensively studied during the last four decades, period-adding and the possibility of other routes to complex oscillations have not yet received much attention. The discovery of period-adding in the Hénon map augments significantly the knowledge about the organization of periodic orbits supported by a popular map that has been under close scrutiny for so long.

An interesting open problem is to study the organizational structure of the branching of attractors and basins as one approaches the Hamiltonian limit. Here we investigated the systematic organization of the attractors having the next-to-largest basins of attraction. But what sort of regular organizations lie beneath the immense set of additional basins which emerge more and more as we march steadily towards $|b| = 1$? How are such organizations interrelated? A startling and enticing theoretical aspect of the Hénon map is the possibility to study the ubiquitous presence of period-adding cascades in a system without critical points [18], the points

invariably used to classify stability properties of dynamical systems [1–4].

Additional interesting open problems are the following. First, to understand the dynamical origin and the differences, if any, that give rise to the nose N and antinose A [11], the two most salient *vertices* [12] located on the outer boundary of the white phase of chaos seen in Fig. 2. Second, to find the reason for the presence of the wide gap seen in Fig. 2 between boxes B2 and B3, and where apparently no stability windows exist. Are such very salient features arising because of an accumulation of stability boundaries? Third, to discover why box B1 in Fig. 3 seems to contain only phases with even periods. Fourth, are there boundary points belonging simultaneously to five distinct stability phases, like the *quint points* recently discovered in a flow governing a driven Belousov–Zhabotinsky reaction [29]?

The Hénon map is analytically tractable to a large extent, and opens the possibility to investigate intricate and unexplored features in both maps and dissipative flows. A deeper understanding of the nested sequences of period-adding stability phases in the Hénon and other maps will likely require new insights on the nature of the towers of algebraic numbers underlying their arithmetic genesis and the nature of the accumulation points generated by them.

Declaration of Competing Interest

Authors declare that they have no conflict of interest.

Acknowledgments

JRBMA thanks CNPq, Brazil, for a doctoral fellowship. JACG was partially supported by CNPq, grant 305305/2020-4. The bitmaps in Figs. 1 and 7 were computed at the CESUP-UFRGS Supercomputer Center of the Federal University in Porto Alegre, Brazil.

References

- [1] Strogatz S. Nonlinear dynamics and chaos with applications to physics, biology, chemistry, and engineering. 2nd ed. Boulder: Westview Press; 2015.
- [2] Argyris J, Faust G, Haase M, Friedrich R. An exploration of dynamical systems and chaos. 2nd ed. New York: Springer; 2015.
- [3] Kautz R. Chaos, the science of predictable random motion. Oxford: Oxford University Press; 2010.
- [4] Hilborn RC. Chaos and nonlinear dynamical systems: an introduction for scientists and engineers. 2nd ed. Oxford: Oxford University Press; 2000.
- [5] van der Pol B, van der Mark J. Frequency demultiplication. Nature 1927;120:363–4.
- [6] Kennedy MP, Chua LO. van der Pol and chaos. IEEE Trans Circ Syst 1986;33:974–80.
- [7] Levi M. A period-adding phenomenon. SIAM J Appl Math 1990;50:943–55.
- [8] Gallas MR, Gallas JAC. Nested arithmetic progressions of oscillatory phases in Olsen's enzyme reaction model. Chaos 2015;25:064603.
- [9] Hauser MJB, Gallas JAC. Nonchaos-mediated mixed-mode oscillations in an enzyme reaction system. J Phys Chem Lett 2014;5:4187–93.
- [10] Gallas JAC, Hauser MJB, Olsen LF. Complexity of a peroxidase-oxidase reaction model. Phys Chem Chem Phys 2021;23:1943–55.
- [11] Gallas JAC. Structure of the parameter space of the Hénon map. Phys Rev Lett 1993;70:2714–17.
- [12] Gallas JAC, Grebogi C, Yorke JA. Vertices in parameter space: double crisis which destroy chaotic attractors. Phys Rev Lett 1993;71:1359–62.
- [13] Pando CL, Meucci R, Ciofini M, Arecchi FT. CO₂ laser with modulated losses: theoretical models and experiments in the chaotic regime. Chaos 1993;3:279–86.
- [14] Pando CL, Acosta GAL, Meucci R, Ciofini M. Highly dissipative Hénon map behavior in the four-level model of the CO₂ laser with modulated losses. Phys Lett A 1995;199:191–8.
- [15] Bonatto C, Garreau JC, Gallas JAC. Self-similarities in the frequency-amplitude space of a loss-modulated CO₂ laser. Phys Rev Lett 2005;95:143905.
- [16] Freire JG, Meucci R, Arecchi FT, Gallas JAC. Self-organization of pulsing and bursting in a CO₂ laser with opto-electronic feedback. Chaos 2015;25:097607. special issue *the 25th anniversary of chaos - perspectives on nonlinear science – past, present, and future*.
- [17] Tramontana F, Gardini L, Avrutin V, Schanz M. Period adding in piecewise linear maps with discontinuities. Int J Bifurc Chaos 2012;22:1250068.
- [18] Endler A, Gallas JAC. Mandelbrot-like sets in dynamical systems with no critical points. Comptes Rendus Math (Paris) 2006;342:681–4.
- [19] Gallas JAC. Spiking systematics in some CO₂ laser models. Adv At Mol Opt Phys 2016;65:127–91.
- [20] Heagy JF. A physical interpretation of the Hénon map. Phys D 1992;57:436–46.
- [21] Lorenz EN. Compound windows of the Hénon map. Phys D 2008;237:1689–704.
- [22] Motter AE, Campbell DK. Chaos at fifty. Phys Today 2013;66:27–33.
- [23] Martins LC, Gallas JAC. Multistability, phase diagrams and statistical properties of the kicked rotor: a map with many coexisting attractors. Int J Bifurc Chaos 2008;18:1705–17.
- [24] Feudel U, Grebogi C, Poon L, Yorke JA. Dynamical properties of a simple mechanical system with a large number of coexisting attractors. Chaos Solitons Fractals 1998;9:171–80.
- [25] Feudel U, Grebogi C, Hunt BR, Yorke JA. Map with more than 100 coexisting low-periodic attractors. Phys Rev E 1996;54:71–81.
- [26] Holmes P, Whitley D. Bifurcation of one- and two-dimensional maps. Philos Trans R Soc A 1984;311:43–102.
- [27] Holmes P. Bifurcation sequences in horseshoe maps: infinitely many routes to chaos. Phys Lett A 1984;104:299–302.
- [28] Ling FH. A numerical method for determining bifurcation curves of mappings. Phys Lett A 1985;110:116–20.
- [29] Field RJ, Freire JG, Gallas JAC. Quint points lattice in a driven Belousov-Zhabotinsky reaction model. Chaos 2021;31:053124.